One-Pot and Template-Free Fabrication of ZnS·(ethylenediamine)0.5 Hybrid Nanobelts

ARTICLE *in* THE JOURNAL OF PHYSICAL CHEMISTRY C · APRIL 2012

Impact Factor: 4.77 · DOI: 10.1021/jp212420x

3 AUTHORS, INCLUDING:

Yeonho Kim
Korea Basic Science Institute KBSI
7 PUBLICATIONS **37** CITATIONS
SEE PROFILE

Jong-Yeob Kim
Seoul National University
13 PUBLICATIONS **132** CITATIONS
SEE PROFILE

THE JOURNAL OF PHYSICAL CHEMISTRY C

Article

pubs.acs.org/JPCC

One-Pot and Template-Free Fabrication of ZnS·(ethylenediamine)$_{0.5}$ Hybrid Nanobelts

Yeonho Kim, Jong-Yeob Kim, and Du-Jeon Jang*

School of Chemistry, Seoul National University, NS60, Seoul 151-747, Republic of Korea

Supporting Information

ABSTRACT: A template-free and one-pot solvothermal process has been developed for the facile synthesis of ZnS·(en)$_{0.5}$ (en = ethylenediamine) hybrid nanobelts having diverse length-to-width (aspect) ratios. While typical hybrid nanobelts synthesized at 180 °C for 6 h have an average width of 130 nm, a mean thickness of 55 nm, and an average length of 16 μm, their aspect ratios have been varied by adjusting solvent volume ratios of hydrazine monohydrate (hm) to en. A sufficient amount of sulfide from the reduction of sulfur by hm has been found to be essential for the efficient anisotropic one-dimensional growth of highly crystalline ZnS·(en)$_{0.5}$ hybrid nanobelts. The photoluminescence spectra of ZnS·(en)$_{0.5}$ hybrid nanostructures exhibit three bands located at 327, 415−430, and 587−654 nm, which are assigned to band-edge emission, trap sites-related emission, and anion-vacancy emission, respectively. The mean lifetime of photoluminescence having three decay components of 30, 170, and 2700 ps decreases with the volume ratio of hm to en due to the decrease of defect sites with the increase of the aspect ratios of ZnS·(en)$_{0.5}$ hybrid nanobelts. Compared with bare-ZnS nanobelts prepared by the hydrothermal treatment of ZnS·(en)$_{0.5}$ hybrid nanobelts, hybrid ones have shown enhanced optical properties that would give them potential for optoelectronic devices.

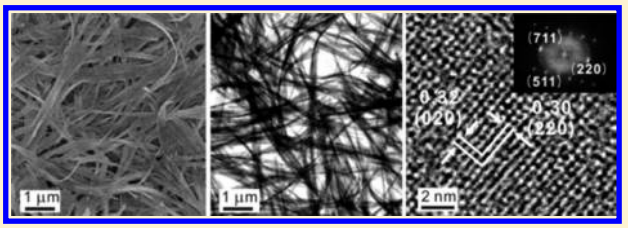

1. INTRODUCTION

The controlled fabrication, characterization, and application of nanometer-sized metals and semiconductors with functional properties have been studied widely.[1−4] In particular, one-dimensional nanoscale building blocks such as nanowires, nanorods, nanotubes, and nanobelts have been investigated extensively because of their potential applications in various fields. Compared with common one-dimensional nanostructures, nanobelts as representative quasi-one-dimensional nanostructures with improved electrical contact have attracted considerable attention due to their proven use as both interconnects and functional units in electronic, optoelectronic, electrochemical, and electromechanical devices.[5−9] ZnS is an important II−VI semiconductor compound with a wide band gap energy of 3.66 eV at room temperature, and it attracts intense interest due to its excellent properties of luminescence which enable ZnS to have applications in the fields of UV-light emitting diodes, efficient phosphors, sensors, and catalysts.[10−14] From the viewpoint of applications, one-dimensional ZnS nanostructures with highly aligned and ordered patterns are in great demand to become the current focus of research and used as building blocks for nanoelectronic and nanophotonic systems because of their enhanced properties significantly different from those of their bulk counterparts.[15] Up to now, different methods such as metal−organic chemical vapor deposition, electrochemical deposition, template assistance, and thermal evaporation have been developed for the synthesis of one-dimensional ZnS nanostructures.[16−18] Commonly, these synthetic strategies need relatively rigid experimental conditions and sophisticated equipments. On the contrary to these, a solution-based approach such as a solvothermal process has advantages of mild synthetic conditions and economical methods for the fabrication of one-dimensional ZnS nanostructures, especially because this approach does not require toxic gases or high-temperature processing steps.[19] However, there are few reports on the synthesis of ZnS nanobelts via a solvothermal process.[20] This may be due to the fact that it is generally difficult to control the nucleation and growth of ZnS for the fabrication of well-defined one-dimensional nanostructures.

Inorganic−organic hybrid materials with one-dimensional structures have received much attention because of their tremendous potential in providing enhanced materials properties that are not easily achievable with either organic or inorganic materials alone.[21] For example, II−VI-based one-dimensional hybrid semiconductors, MQ−(L)$_n$ (M = Zn, Cd, Mn; Q = S, Se, Te; L = hydrazine, ethylenediamine (en), cyclohexylamine; n = 0.5 or 1) have been demonstrated to be a new family of multifunctional hybrid materials.[21−24] These hybrid materials normally exhibit tunable physical properties and significantly enhanced electronic and optical properties including a giant band gap tunability as a result of strong quantum confinement effect and high band-edge absorption. The hybrid materials have the additional advantage of possessing perfectly ordered crystal structures and thus allowing high carrier mobility. Furthermore, the hybrid materials are

Received: December 23, 2011
Revised: April 24, 2012
Published: April 24, 2012

dx.doi.org/10.1021/jp212420x | J. Phys. Chem. C 2012, 116, 10296−10302

much lighter and more flexible compared with their inorganic counterparts, and thus are most desirable for low-weight and flexible electronic devices. Because hybrid materials with one-dimensional structures are remarkably advantageous, there have been many corresponding works on the ZnS-based hybrid nanostructures.[25−29] Although the preparation of $ZnS{\cdot}(en)_{0.5}$ hybrid nanosheets was already reported, the synthesis and characterization of $ZnS{\cdot}(en)_{0.5}$ hybrid nanobelts have hardly been reported.[25] Many researchers have used ethylenediamine (en) as organic spacer molecules or template molecules for the synthesis of II−VI-based one-dimensional hybrid semiconductors. And, en molecules, which serve as bridged ligands between two metal atoms in neighboring inorganic layers, also prevent these inorganic slabs from collapsing and condensing into the bulk phase. A solvent coordination molecular template mechanism was already proposed with an emphasis on the role of the en molecule in assisting the anisotropic crystal growth.[30]

In this paper, we report a template-free and one-pot solvothermal process for the synthesis of $ZnS{\cdot}(en)_{0.5}$ hybrid nanobelts having diverse length-to-width (aspect) ratios. Hybrid nanobelts with distinct three emission bands have been prepared by a facile solvothermal route in a mixed solvent system containing a variable volume ratio of hydrazine monohydrate (hm) to en. The reaction medium consisting of mixed solvents has played an important role in the morphology and crystallinity of the nanostuctures. As-synthesized hybrid nanobelts show different optical properties compared with bare-ZnS nanobelts fabricated by a hydrothermal treatment of $ZnS{\cdot}(en)_{0.5}$ hybrid nanobelts. The photoluminescence properties, as well as the crystallinity and size, of $ZnS{\cdot}(en)_{0.5}$ hybrid nanostructures can be varied by adjusting volume ratios of hm to en without changing precursor molecules and without doping impurities. Thus, the simple and mild solution approach to synthesize inorganic−organic hybrid nanobelts with obvious advantages over the traditional high-temperature approach could be applicable to other II−VI semiconductor nanomaterials. Furthermore, our fabrication method of $ZnS{\cdot}(en)_{0.5}$ hybrid nanobelts with controlled structures and improved optical properties is considered to enhance their potential application as nanoscale optoelectronic devices and catalysts in pollutant treatment.

2. EXPERIMENTAL SECTION

Synthesis. The analytical grade chemicals of $ZnCl_2$(s), S(s), $N_2H_4{\cdot}H_2O$(l,hm), and $C_2H_4(NH_2)_2$(l,en) were used as purchased from Sigma-Aldrich. Deionized water with a resistivity of greater than 18 MΩ cm, from a Millipore Milli-Q system, was used throughout the experiments. For the typical preparation of $ZnS{\cdot}(en)_{0.5}$ hybrid nanostructures, 0.5 mmol of $ZnCl_2$, 0.5 mmol of S, and a volume (7.5, 15.0, or 20.0 mL) of en (V_{en}) were added to a volume of hm (V_{hm} = 30.0 mL − V_{en}) and stirred vigorously for 1 h. The mixture solution was then loaded into a Teflon-lined stainless-steel autoclave of 50 mL capacity, placed in a preheated oven at 180 °C for 6 h, and cooled to room temperature naturally. A white precipitate produced in the reaction mixture was washed twice with deionized water and ethanol to remove residual impurities. Bare-ZnS nanobelts were then fabricated by treating $ZnS{\cdot}(en)_{0.5}$ hybrid nanobelts hydrothermally for 10 h at 120 °C in a Teflon-lined stainless-steel autoclave. Colloidal samples were prepared by redispersing the prepared hybrid nanostructures in deionized water immediately prior to use in order to avoid the precipitation and the decomposition of nanostructures in water.

Characterization. While transmission electron microscopy (TEM) images were obtained with a Hitachi H-7600 microscope, high-resolution transmission electron microscopy (HRTEM) images and fast Fourier transformation (FFT) patterns were measured using a JEOL JEM-3000F microscope. Scanning electron microscopy (SEM) images were obtained with a JEOL-6700F microscope, and high-resolution X-ray diffraction (HRXRD) patterns were obtained with a Bruker D8 DISCOVER diffractometer using Cu Kα radiation (0.15418 nm). X-ray photoelectron spectroscopy (XPS) spectra were monitored using a AXIS-His system with an excitation source of Mg Kα (1253.60 eV), and Raman spectra were measured with a HORIABA Jobin Yvon T64000 spectrometer with excitation using 514 nm light from an Ar^+ laser. While extinction spectra were obtained with a Scinco S3100 UV/vis spectrophotometer, photoluminescence spectra were measured employing a Princeton Instruments ICCD576G CCD detector with excitation using 266-nm pulses having a duration time of 6 ns from a Q-switched Quantel Brilliant Nd:YAG laser. Photoluminescence kinetic profiles were measured using a Hamamatsu C2830 streak camera of 10 ps attached with a Princeton Instruments RTE128H CCD detector after exciting samples with 266 nm pulses from a mode-locked Quantel YG501 Nd:YAG laser of 25 ps. Photoluminescence kinetic constants were extracted by fitting measured kinetic profiles to computer-simulated exponential curves convoluted with instrument response functions.

3. RESULTS AND DISCUSSION

The SEM and TEM images of Figure 1a show that syntheses performed with V_{hm}/V_{en} of 3 give nanobelts having well-defined uniform widths over their entire lengths, with an average width of 130 nm, a mean thickness of 55 nm, and a typical length of 16 μm. It will be shown later that these products are $ZnS{\cdot}(en)_{0.5}$ hybrid nanobelts. The comparison of the SEM and TEM images in Figure 1 reveals that the lengths of the nanostructures have increased whereas their widths have decreased with the increment of V_{hm}/V_{en}. Thus, the aspect ratios of $ZnS{\cdot}(en)_{0.5}$ hybrid nanostructures increase with the increment of V_{hm}/V_{en}. These results suggest that the mixed solvent system containing hm and en has played an important role in the morphology of the nanostructures. On the basis of our experimental data, we suggest that a large value of V_{hm}/V_{en} has been found to be essential for the growth of flexible and well-defined $ZnS{\cdot}(en)_{0.5}$ hybrid nanobelts. Therefore, an excess amount of en and an insufficient amount of sulfide ions (see below) induce nanostructures to grow with small aspect ratios.

The microstructural details of $ZnS{\cdot}(en)_{0.5}$ hybrid nanostructures have been further provided by measuring the HRTEM images and the FFT patterns of Figure 2. The HRTEM images of Figure 2 show that the hybrid nanobelt synthesized with V_{hm}/V_{en} of 3 has a single-domain crystallite whereas hybrid nanostructures synthesized with V_{hm}/V_{en} of 1 and 0.5 have multidomain crystallites. These are also clearly seen from the FFT patterns of Figure 2. Comparing the inset of Figure 2a with those of parts b and c of Figure 2, we can observe that the number of discrete spots increases with the increment of V_{hm}/V_{en}. In other words, ring FFT patterns due to polycrystalline structures have appeared when nanosheets were grown with V_{hm}/V_{en} of 1 and 0.5, and discrete spots have evolved to exist when hybrid nanobelts were grown with V_{hm}/V_{en} of 3. The

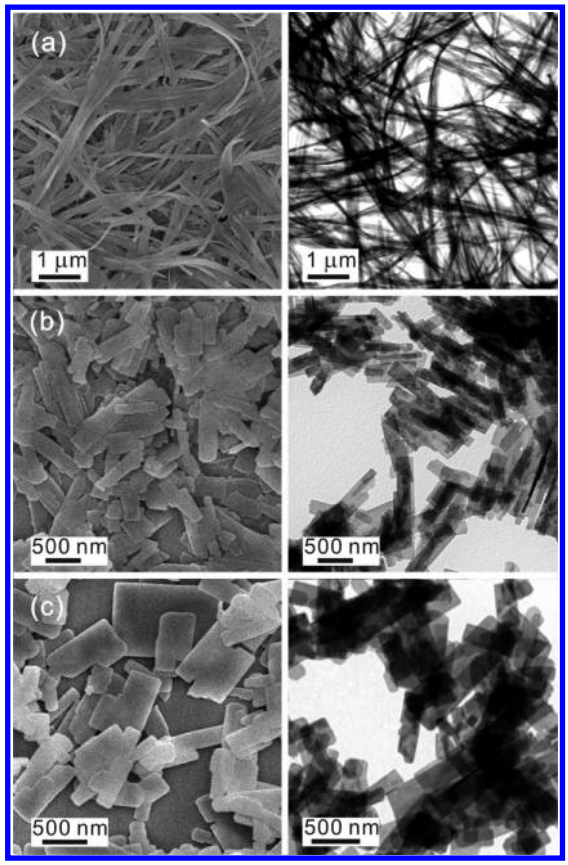

Figure 1. SEM (left) and TEM (right) images of $ZnS{\cdot}(en)_{0.5}$ nanostructures grown at 180 °C for 6 h with V_{hm}/V_{en} of 3 (a), 1 (b), and 0.5 (c).

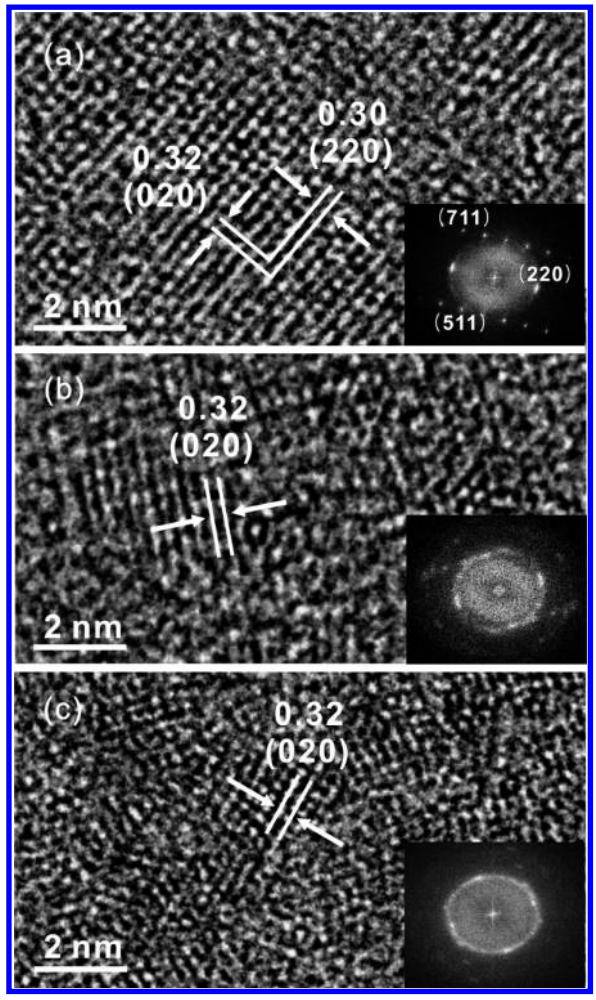

Figure 2. HRTEM images of $ZnS{\cdot}(en)_{0.5}$ nanostructures grown at 180 °C for 6 h with V_{hm}/V_{en} of 3 (a), 1 (b), and 0.5 (c) show lattice plane distances in nm. The insets show FFT patterns obtained from the corresponding nanostructures.

lattice-fringe distances of 0.30 and 0.32 nm calculated from the HRTEM images of Figure 2 have been assigned to the spacing lengths of the (220) and the (020) planes, respectively, of the orthorhombic $ZnS{\cdot}(en)_{0.5}$ structure. The typical FFT pattern of Figure 2a also suggests that the nanobelt has the crystalline structure of the orthorhombic $ZnS{\cdot}(en)_{0.5}$. Consequently, both the HRTEM image and the FFT pattern of Figure 2a indicate that a $ZnS{\cdot}(en)_{0.5}$ hybrid nanobelt fabricated with V_{hm}/V_{en} of 3 shows a well-defined and single-crystalline structure.

Figure 3 shows the HRXRD patterns of $ZnS{\cdot}(en)_{0.5}$ hybrid nanostructures as-prepared via a solvothermal process with different reaction conditions of time and V_{hm}/V_{en}. The 2θ positions and the relative intensities of our observed reflection peaks are in good agreement with the respective ones of $ZnS{\cdot}(en)_{0.5}$ nanostructures reported in the literature,[31,33−35] indicating that $ZnS{\cdot}(en)_{0.5}$ hybrid nanostructures have been successfully synthesized under current experimental conditions. It is suggested that our en-intercalated ZnS hybrid nanostructures of $ZnS{\cdot}(en)_{0.5}$ have lamellalike structures with ZnS nanolayers ordered via bridging en spacers.[31] The HRXRD patterns of Figure 3a designate that the crystallinity of $ZnS{\cdot}(en)_{0.5}$ hybrid nanobelts has enhanced highly with the increment of the reaction time. This suggests that a sufficient reaction time as long as 6 h is essential for the growth of well-defined and high-crystalline $ZnS{\cdot}(en)_{0.5}$ hybrid nanobelts. The mean crystallite diameter, d, can be determined from the line width of a HRXRD spectrum by the Scherrer's formula $\langle d\rangle = (0.94\ \lambda)/(B\cos\ \theta_B)$, where λ is the X-ray wavelength, B is the full width at the half-maximum of the diffraction peak (radian), and θ_B is the half angle of the diffraction peak on the 2θ scale.[36] The mean crystallite diameters of $ZnS{\cdot}(en)_{0.5}$ hybrid nanobelts grown for 3 and 6 h, estimated by using the peak at 2θ of 42°, are 26 and 28 nm, respectively. The peak at 42° has been assigned to the (711) or (620) direction,[31,33] thus suggesting that $ZnS{\cdot}(en)_{0.5}$ hybrid nanobelts grow preferentially in the direction of (711) or (620) to induce an anisotropic one-dimensional growth of nanobelts. Figure 3b shows that broad HRXRD peaks have been induced by the increment of V_{hm}/V_{en}. The relatively broad HRXRD peaks reveal that the average crystallite size of the $ZnS{\cdot}(en)_{0.5}$ hybrid nanostructures has decreased with the increment of V_{hm}/V_{en}. The mean crystallite diameters of $ZnS{\cdot}(en)_{0.5}$ hybrid nanostructures have been estimated to be 28, 49, and 55 nm at V_{hm}/V_{en} values of 3, 1, and 0.5, respectively. The HRXRD patterns of nanostructures in Figure 3b are nearly independent of the V_{hm}/V_{en} ratio. This indicates that both the compositions and the microscopic structures of as-prepared $ZnS{\cdot}(en)_{0.5}$ are the same regardless of V_{hm}/V_{en}, which, however, has changed the aspect ratios of $ZnS{\cdot}(en)_{0.5}$ nanocomposites significantly (Figures 1 and 2). The Raman peaks of Figure S1 of Supporting Information at 216 and 284 cm^{-1} are attributed to a longitudinal acoustic mode and a transverse optic mode of $ZnS{\cdot}(en)_{0.5}$ hybrid nanostructures, respectively.[37] The positions and relative

dx.doi.org/10.1021/jp212420x | J. Phys. Chem. C 2012, 116, 10296−10302

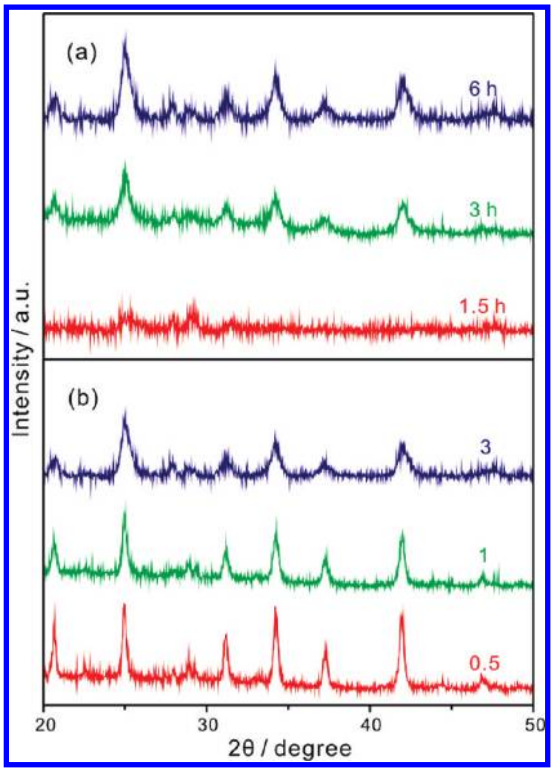

Figure 3. HRXRD patterns of $ZnS{\cdot}(en)_{0.5}$ nanostructures grown at 180 °C with V_{hm}/V_{en} of 3 during various *reaction* periods indicated inside (a) and for 6 h with various ratios of V_{hm}/V_{en} indicated inside (b).

intensities of both peaks do not change with V_{hm}/V_{en}. Thus, together with Figure 3b, Figure S1 of Supporting Information suggests that the microscopic structures of $ZnS{\cdot}(en)_{0.5}$ nanocomposites are almost identical regardless of V_{hm}/V_{en}. The sharp and strong diffraction peaks appearing in the HRXRD patterns of Figure 3 indicate clearly that well-crystallized $ZnS{\cdot}(en)_{0.5}$ hybrid nanostructures have been successfully synthesized via our one-pot and template-free solvothermal process.

The XPS data of Figure 4 can provide further significant information about the surface composition of the $ZnS{\cdot}(en)_{0.5}$ hybrid nanobelts. The binding energies obtained in the XPS analysis were corrected for specimen charging, through referencing the C 1s to 283.5 eV. The survey spectrum of Figure 4a shows that N and C, as well as Zn and S, are present in the hybrid nanobelts. The presence of N and C in the survey spectrum is due to the coordinated organic spacer molecule of en. As shown in Figure 4b, the binding energies of Zn $2p_{3/2}$ and Zn $2p_{1/2}$ were identified at 1019.8 and 1042.8 eV, respectively. The XPS data of Figure 4c yield two distinct bands by the Gaussian fitting of the S 2p, and the deconvoluted binding energies of 159.8 and 161.0 eV could be assigned to the S $2p_{3/2}$ and S $2p_{1/2}$ of a Zn−S bond, respectively. The binding energy of N 1s located at 398.4 eV in Figure 4d could be attributed to a Zn−N bond. These XPS results are in good agreement with those in previous reports.[38−40] The binding energy of the Zn−N bond is considered to derive from a derivative of Zn and en such as $Zn{\cdot}(en)_{0.5}^{2+}$. This Zn−N bond in the XPS analysis clearly indicates the existence of organic spacer molecules that are intercalated inside the ZnS structure. In addition, the extinction spectrum of Figure S2 of Supporting Information shows a sharp absorption peak at 262 nm, which corresponds

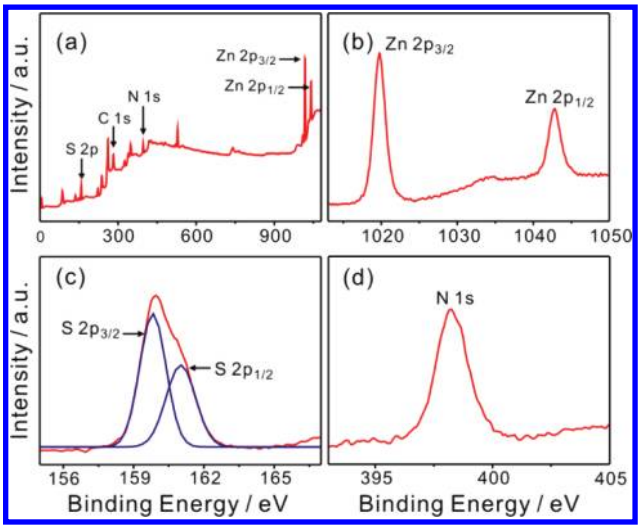

Figure 4. Complete survey (a), Zn 2p (b), S 2p (c), and N 1s (d) XPS spectra of $ZnS{\cdot}(en)_{0.5}$ nanobelts grown at 180 °C for 6 h with V_{hm}/V_{en} of 3.

to 4.73 eV. The peak is largely blue-shifted compared with the absorption peak of bulk ZnS at 335 nm.[19,45] This drastically blue-shifted extinction peak of the $ZnS{\cdot}(en)_{0.5}$ hybrid nanobelts is due to the characteristics of inorganic−organic hybrid nanomaterials.[26,41]

Considering the HRXRD patterns of Figure 3, the XPS spectra of Figure 4, and the extinction spectrum of Figure S2 of Supporting Information, we suggest that our as-synthesized products have the inorganic−organic hybrid nanostructures of $ZnS{\cdot}(en)_{0.5}$. The formation mechanism of our $ZnS{\cdot}(en)_{0.5}$ hybrid nanobelts can be proposed as follows. An en molecule provides a pair of binding sites for a Zn^{2+} ion to produce a chemically stable complex of $Zn{\cdot}(en)_{0.5}^{2+}$ (eq 1). Hydrazine monohydrate (hm) acts as a strong reducing agent of sulfur to form a sulfide ion (S^{2-}); elemental sulfur powder is soluble in hm and a hydrazinium ($N_2H_5^+$) ion can reduce sulfur to a sulfide ion (eqs 2 and 3). The reduced sulfide ion would react with $Zn{\cdot}(en)_{0.5}^{2+}$ to form $ZnS{\cdot}(en)_{0.5}$ (eq 4).[26−28,34,35] The overall reactions can be expressed as follows

$$2Zn^{2+} + en \rightarrow 2Zn{\cdot}(en)_{0.5}^{2+} \quad (1)$$

$$N_2H_4{\cdot}H_2O \rightarrow N_2H_5^+ + OH^- \quad (2)$$

$$N_2H_5^+ + 2S + 5OH^- \rightarrow N_2 + 2S^{2-} + 5H_2O \quad (3)$$

$$Zn{\cdot}(en)_{0.5}^{2+} + S^{2-} \rightarrow ZnS{\cdot}(en)_{0.5} \quad (4)$$

The complexing reagent of en, which contains a pair of chelating N atoms in each molecule, possibly combines with Zn^{2+} and S^{2-} in a line owing to its linear structure. On the other hand, a sufficient amount of hm, a large value of V_{hm}/V_{en}, facilitates the formation of active S^{2-} through an interfacial process, providing a large quantity of excess S^{2-} ions in the reaction mixture. This is believed to be the driving force for the efficient growth of one-dimensional $ZnS{\cdot}(en)_{0.5}$ hybrid nanobelts. It has been reported that if a reaction with two precursors is employed to synthesize semiconductor nanostructures, an excess of the relatively less reactive precursor generates elongated nanostructures with higher aspect ratios.[42] In our experiment, a large excess of S^{2-} provided from the reduction of S by hm at a large value of V_{hm}/V_{en} is the kinetic driving force

dx.doi.org/10.1021/jp212420x | J. Phys. Chem. C 2012, 116, 10296−10302

for the anisotropic one-dimensional growth of $ZnS{\cdot}(en)_{0.5}$ hybrid nanostructures.

The comparative study of the optical properties of nanostructures is helpful to evaluate the quality of product materials and can shed light on their potential applications. The photoluminescence spectra of Figure 5, as well as the extinction spectrum of Figure S2 of Supporting Information, show that $ZnS{\cdot}(en)_{0.5}$ hybrid nanostructures have different optical features compared with not only bulk ZnS but also bare-ZnS nanobelts, due to the characteristics of inorganic–organic hybrid nanomaterials.[20,26,41,43] Room-temperature photoluminescence spectra of $ZnS{\cdot}(en)_{0.5}$ hybrid nanostructures are shown in Figure 5. Each of the curves exhibits three bands located at 327, 415–430, and 587–654 nm, which can be assigned to UV, blue, and orange emission bands, respectively. The first UV emission band located at 327 nm should be attributed to the band-edge emission of $ZnS{\cdot}(en)_{0.5}$ hybrid nanostructures. Although the large exciton-binding energy (40 meV) is much higher than thermal energy at room temperature (about 25 meV), the band-edge emission can be observed only in very high-quality single nanocrystals at room temperature.[44] Thus, the observed band-edge emission indicates that $ZnS{\cdot}(en)_{0.5}$ hybrid nanobelts synthesized with V_{hm}/V_{en} of 3 are highly crystalline. This is consistent with the results discussed with the HRTEM image and the FFT pattern of Figure 2a. To the best of our knowledge, this strong band-edge emission has been hardly reported for ZnS nanobelts synthesized via solution approaches.[10,45] The second blue emission band centered at 415–430 nm, originating from trap sites or surface states,[41,46,47] shifts gradually to the blue by 15 nm with the increase of V_{hm}/V_{en}. This blue shift has been attributed to enhanced quantum confinement due to the decreased average crystallite size[21] of $ZnS{\cdot}(en)_{0.5}$ hybrid nanostructures with the increment of V_{hm}/V_{en}, as discussed with Figure 3b. The photoluminescence intensity of $ZnS{\cdot}(en)_{0.5}$ hybrid nanobelts synthesized with V_{hm}/V_{en} of 3 is stronger by 50% than that of $ZnS{\cdot}(en)_{0.5}$ hybrid nanosheets synthesized with V_{hm}/V_{en} of 0.5 or 1. This intensity increase has been ascribed to the decrease of defect sites owing to crystallinity increase as discussed with Figure 2, as well as the decrease of surface states due to aspect ratios increase as shown in Figure 1, with the increase of V_{hm}/V_{en}. The last orange emission band centered at 587–654 nm has been attributed to arise from two kinds of anion (sulfide) vacancies capturing two electron (F-centers) or one electron (F^+-centers).[48] Figure S3 of Supporting Information shows that the orange emission band can be deconvoluted into an emission band of F^+-centers at 586–591 nm and an emission band of F-centers at 654–655 nm. The contribution of the orange emission in total photoluminescence decreases significantly with the increase of V_{hm}/V_{en}. This has also been ascribed to the decrease of defect sites due to crystallinity increase with the increment of V_{hm}/V_{en} as discussed with Figure 2. Because hm acts as a strong reducing agent of S to form S^{2-} (see above), the amount of defect sites, which are anion vacancies, decreases with the increment of V_{hm}/V_{en}.

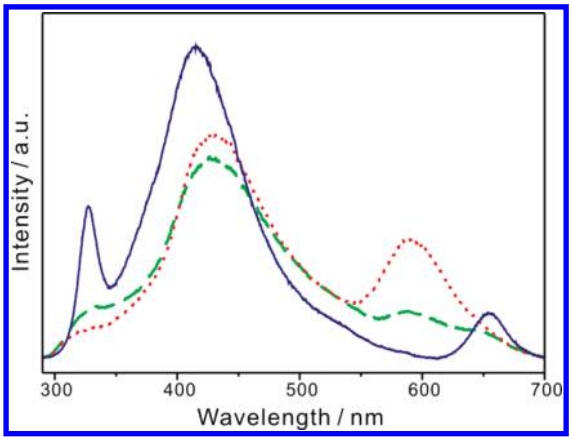

Figure 5. Photoluminescence spectra of $ZnS{\cdot}(en)_{0.5}$ nanostructures grown at 180 °C for 6 h with V_{hm}/V_{en} of 3 (solid), 1 (dashed), and 0.5 (dotted). The nanostructures were suspended in water and excited with 266-nm laser pulses of 6 ns.

Figure 6 and Table 1 indicate that the photoluminescence kinetic profiles of $ZnS{\cdot}(en)_{0.5}$ hybrid nanostructures look similar to one another with having three decay components although their mean emission lifetime decreases with the increase of V_{hm}/V_{en}. The decrease of the mean emission lifetime with the increment of V_{hm}/V_{en} is considered to associate with the decrease of defect sites or surface states as described with Figure 5. The fast decay time of 30 ps is considered to be the trapping time of electrons in the conduction band of $ZnS{\cdot}(en)_{0.5}$ hybrid nanostructures while the medium decay time of 170 ps is attributed to the relaxation time of electrons at trap sites via being trapped into surface states. We have then assigned the slow decay time of 2700 ps to the hole recombination time of electrons at surface states. While the decreasing amplitude of the medium decay component with the increase of V_{hm}/V_{en} can be attributed to the decrease of defect sites owing to crystallinity increase as

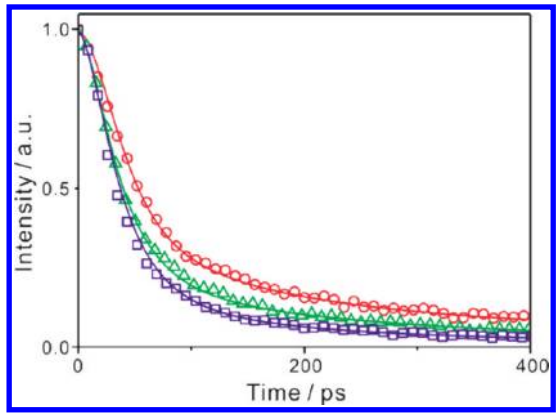

Figure 6. Maximum-normalized photoluminescence decay kinetic profiles of $ZnS{\cdot}(en)_{0.5}$ nanostructures grown at 180 °C for 6 h with V_{hm}/V_{en} of 3 (squares), 1 (triangles), and 0.5 (circles) suspended in water. Photoluminescence was monitored at 450 nm after excitation with 266-nm pulses of 25 ps. Solid lines are the best-fitted curves to extract lifetimes given in Table 1.

Table 1. Photolumeniscence Decay Kinetic Constants of $ZnS{\cdot}(en)_{0.5}$ Nanostructures Suspended in Water[a]

V_{hm}/V_{en}	lifetime/ps	mean lifetime/ps
3.0	30 (91.5%) + 170 (7.5%) + 2700 (1.0%)[b]	67
1.0	30 (87.0%) + 170 (11.0%) + 2700 (2.0%)	99
0.5	30 (82.7%) + 170 (14.5%) + 2700 (2.8%)	125

[a]Deconvoluted from the kinetic profiles of Figure 6. [b]Initial intensity percentage of each component.

dx.doi.org/10.1021/jp212420x | J. Phys. Chem. C 2012, 116, 10296–10302

discussed with Figure 2, the amplitude decrease of the slow component is ascribed to the decrease of surface states due to size increase with V_{hm}/V_{en} as shown in Figure 1.

The decay profile of the orange emission band at 584−654 nm has been found to be too slow to be observed with our picosecond kinetic spectrometer because radiative transition from the relaxed excited state (2s) to the ground state (1s) of F-centers is not allowed by the spectroscopic selection rule of Laporte. Figure S6 of Supporting Information suggests that the photoluminescence spectrum of en-removed bare-ZnS nanobelts is substantially different from that of $ZnS{\cdot}(en)_{0.5}$ hybrid nanobelts. While hydrothermal treatment has reduced UV band-edge emission substantially, it has removed orange F-center emission drastically. Figure S6 of Supporting Information also shows that hydrothermal treatment shifts both the UV and the blue emission bands of $ZnS{\cdot}(en)_{0.5}$ hybrid nanobelts to the red by 8 nm. This suggests that the band gap of $ZnS{\cdot}(en)_{0.5}$ hybrid nanobelts is higher than that of bare-ZnS nanobelts. Compared with bare-ZnS nanobelts, $ZnS{\cdot}(en)_{0.5}$ hybrid nanobelts have shown enhanced optical properties that would give them potential for nanoscale optoelectronic devices.

4. CONCLUSIONS

Flexible and well-defined $ZnS{\cdot}(en)_{0.5}$ (en = ethylenediamine) hybrid nanobelts with high aspect ratios have been facilely synthesized by a template-free and one-pot solvothermal process. The appearance structures, crystallite sizes, and optical properties of $ZnS{\cdot}(en)_{0.5}$ hybrid nanostructures can be tuned by modifying the volume ratio (V_{hm}/V_{en}) of hydrazine monohydrate (hm) to en. Hybrid nanobelts having single-domain crystallites have been synthesized with V_{hm}/V_{en} of 3 while hybrid nanosheets having multidomain crystallites have been synthesized with V_{hm}/V_{en} of 0.5 or 1. A reaction time as long as 6 h has been found to be essential for the growth of highly crystalline $ZnS{\cdot}(en)_{0.5}$ hybrid nanobelts. A sufficient amount of hm, i.e., a large value of V_{hm}/V_{en}, facilitates the abundant formation of active S^{2-} through an interfacial process, suggesting that a large quantity of excess S^{2-} ions in the reaction mixture is the driving force for the efficient growth of anisotropic one-dimensional $ZnS{\cdot}(en)_{0.5}$ hybrid nanobelts. $ZnS{\cdot}(en)_{0.5}$ hybrid nanostructures exhibit three emission bands: band-edge emission at 327 nm, trap sites-related emission at 415−430 nm, and anion (sulfide)-vacancy emission at 584−654 nm. The spectral properties of three bands are affected by the crystallinity and size of $ZnS{\cdot}(en)_{0.5}$ hybrid nanostructures, which can be varied by adjusting V_{hm}/V_{en}. The mean lifetime of photoluminescence having three decay components of 30, 170, and 2700 ps decreases with V_{hm}/V_{en} due to the decrease of defect sites with the increase of the aspect ratios of $ZnS{\cdot}(en)_{0.5}$ hybrid nanobelts. We have also shown that the organic molecules of $ZnS{\cdot}(en)_{0.5}$ hybrid nanobelts can be removed via a relatively mild hydrothermal treatment process to fabricate bare-ZnS nanobelts.

■ ASSOCIATED CONTENT

Supporting Information

Raman spectra, extinction spectrum, additional photoluminescence spectra, additional HRXRD patterns, and additional TEM image. This material is available free of charge via the Internet at http://pubs.acs.org.

■ AUTHOR INFORMATION

Corresponding Author

*E-mail: djjang@snu.ac.kr. Tel: +82-(2)-880-4368. Fax: +82-(2)-875-6624.

Notes

The authors declare no competing financial interest.

■ ACKNOWLEDGMENTS

This work was supported by the National Research Foundation of Korea grant funded by the Korea government (MEST) (2011-0028981 and 2007−0056331).

■ REFERENCES

(1) Pan, Z. W.; Dai, Z. R.; Wang, Z. L. *Science* **2001**, *291*, 1947−1949.
(2) Liu, B.; Bando, Y.; Jiang, X.; Li, C.; Fang, X.; Zeng, H.; Terao, T.; Tang, C.; Mitome, M.; Golberg, D. *Nanotechnology* **2010**, *21*, 375601.
(3) Che, Y.; Datar, A.; Balakrishnan, K.; Zang, L. *J. Am. Chem. Soc.* **2007**, *129*, 7234−7235.
(4) Kim, J.-Y.; Kim, S. J.; Jang, D.-J. *J. Phys. Chem. C* **2011**, *115*, 672−675.
(5) Joo, J.; Son, J. S.; Kwon, S. G.; Yu, J. H.; Hyeon, T. *J. Am. Chem. Soc.* **2006**, *128*, 5632−5633.
(6) Kim, J.-Y.; Jeong, H.; Jang, D.-J. *J. Nanopart. Res.* **2011**, *13*, 6699−6706.
(7) Yin, L.; Bando, Y. *Nat. Mater.* **2005**, *4*, 883−884.
(8) Gong, J.; Yang, S.; Duan, J.; Zhang, R.; Du, Y. *Chem. Commun.* **2005**, 351−353.
(9) Che, Y.; Datar, A.; Yang, X.; Naddo, T.; Zhao, J.; Zang, L. *J. Am. Chem. Soc.* **2007**, *129*, 6354−6355.
(10) Chen, R.; Li, D.; Liu, B.; Peng, Z.; Gurzadyan, G. G.; Xiong, Q.; Sun, H. *Nano Lett.* **2010**, *10*, 4956−4961.
(11) Gautam, U. K.; Fang, X.; Bando, Y.; Zhan, J.; Golberg, D. *ACS Nano* **2008**, *2*, 1015−1021.
(12) Nicolau, Y. F.; Dupuy, M.; Brunel, M. *J. Electrochem. Soc.* **1990**, *137*, 2915−2924.
(13) Fujiwara, H.; Hosokawa, H.; Murakoshi, K.; Wada, Y.; Yanagida, S. *Langmuir* **1998**, *14*, 5154−5159.
(14) Yin, H.; Wada, Y.; Kitamura, T.; Yanagida, S. *Environ. Sci. Technol.* **2001**, *35*, 227−231.
(15) Moore, D. F.; Ding, Y.; Wang, Z. L. *J. Am. Chem. Soc.* **2004**, *126*, 14372−14373.
(16) Zhai, T.; Gu, Z.; Ma, Y.; Yang, W.; Zhao, L.; Yao, J. *Mater. Chem. Phys.* **2006**, *100*, 281−284.
(17) Xu, X.-J.; Fei, G.-T.; Yu, W.-H.; Wang, X.-W.; Chen, L.; Zhang, L.-D. *Nanotechnology* **2006**, *17*, 426−429.
(18) Ma, C.; Moore, D.; Li, J.; Wang, Z. L. *Adv. Mater.* **2003**, *15*, 228−231.
(19) Chai, L.; Du, J.; Xiong, S.; Li, H.; Zhu, Y.; Qian, Y. *J. Phys. Chem. C* **2007**, *111*, 12658−12662.
(20) Yao, W.-T.; Yu, S.-H.; Pan, L.; Li, J.; Wu, Q.-S.; Zhang, L.; Jiang, J. *Small* **2005**, *1*, 320−325.
(21) Kim, J.-Y.; Kim, M. R.; Park, S.-Y.; Jang, D.-J. *CrystEngComm.* **2010**, *12*, 1803−1808.
(22) Huang, X.; Li, J. *J. Am. Chem. Soc.* **2000**, *122*, 8789−8790.
(23) Yao, W.; Yu, S.-H.; Huang, X.; Jiang, J.; Zhao, L. Q.; Pan, L.; Li, J. *Adv. Mater.* **2005**, *17*, 2799−2802.
(24) Deng, Z.-X.; Li, L.; Li, Y. *Inorg. Chem.* **2003**, *42*, 2331−2341.
(25) Zhang, L.; Yang, H.; Li, L.; Zhang, R.; Liu, R.; Ma, J.; Xie, X.; Gao, F. *Inorg. Chem.* **2008**, *47*, 11950−11957.
(26) Yu, S.-H.; Yoshimura, M. *Adv. Mater.* **2002**, *14*, 296−300.
(27) Xi, G.; Wang, C.; Wang, X.; Zhang, Q.; Xiao, H. *J. Phys. Chem. C* **2008**, *112*, 1946−1952.
(28) Ni, Y.; Cao, X.; Hu, G.; Yang, Z.; Wei, X.; Chen, Y.; Xu, J. *Cryst. Growth Des.* **2007**, *7*, 280−285.
(29) Mosca, R.; Ferro, P.; Calestani, D.; Nasi, L.; Besagni, T.; Licci, F. *Cryst. Res. Technol.* **2011**, *46*, 818−822.

(30) Li, Y.; Liao, H.; Ding, Y.; Fan, Y.; Zhang, Y.; Qian, Y. *Inorg. Chem.* **1999**, *38*, 1382−1387.
(31) Ouyang, X.; Tsai, T.-Y.; Chen, D.-H.; Huang, Q.-J.; Cheng, W.-H.; Clearfield, A. *Chem. Commun.* **2003**, 886−887.
(32) Dong, C. *J. Appl. Cryst.* **1999**, *32*, 838.
(33) Zhao, G.-T.; Wang, X.; Yu, J. C. *Cryst. Growth Des.* **2005**, *5*, 1761−1765.
(34) Li, Y.; Ding, Y.; Wang, Z. *Adv. Mater.* **1999**, *11*, 847−850.
(35) Shi, L.; Xu, Y.; Li, Q. *Cryst. Growth Des.* **2009**, *9*, 2214−2219.
(36) Bandaranayake, R. J.; Wen, G. W.; Lin, L. Y.; Jiang, H. X.; Sorensen, C. M. *Appl. Phys. Lett.* **1995**, *67*, 831−833.
(37) Xiong, Q.; Wang, J.; Reese, O.; Voon, L. C. L. Y.; Eklund, P. C. *Nano Lett.* **2004**, *4*, 1991−1996.
(38) Ahmad, M.; Yan, X.; Zhu, J. *J. Phys. Chem. C* **2011**, *115*, 1831−1837.
(39) Kim, D.-P.; Kim, C.-I.; Kwon, K.-H. *Thin Solid Films* **2004**, *459*, 131−136.
(40) Cao, P.; Zhao, D. X.; Zhang, J. Y.; Shen, D. Z.; Lu, Y. M.; Yao, B.; Li, B. H.; Bai, Y.; Fan, X. W. *Appl. Surf. Sci.* **2008**, *254*, 2900−2904.
(41) Yu, S.-H.; Yang, J.; Qian, Y.-T.; Yoshimura, M. *Chem. Phys. Lett.* **2002**, *361*, 362−366.
(42) Peng, X. *Adv. Mater.* **2003**, *15*, 459−463.
(43) Huang, X.; Li, J.; Zhang, Y.; Mascarenhas, A. *J. Am. Chem. Soc.* **2003**, *125*, 7049−7055.
(44) Tran, T. K.; Park, W.; Tong, W.; Kyi, M. M.; Wagner, B. K.; Summers, C. J. *J. Appl. Phys.* **1997**, *81*, 2803−2809.
(45) Fang, X.; Bando, Y.; Liao, M.; Gautam, U. K.; Zhi, C.; Dierre, B.; Liu, B.; Zhai, T.; Sekiguchi, T.; Koide, Y.; Golberg, D. *Adv. Mater.* **2009**, *21*, 2034−2039.
(46) Zhu, Y.-C.; Bando, Y.; Xue, D.-F. *Appl. Phys. Lett.* **2003**, *82*, 1769−1771.
(47) Denzler, D.; Olschewski, M.; Sattler, K. *J. Appl. Phys.* **1998**, *84*, 2841−2845.
(48) Harker, A. H. *J. Phys. C* **1978**, *11*, 1059−1065.